Charge confinements in CdSe–ZnSe symmetric double quantum wells

2008 J. Phys.: Condens. Matter 20 165205

(http://iopscience.iop.org/0953-8984/20/16/165205)

IOP PUBLISHING JOURNAL OF PHYSICS: CONDENSED MATTER

J. Phys.: Condens. Matter **20** (2008) 165205 (10pp) doi:10.1088/0953-8984/20/16/165205

Charge confinements in CdSe–ZnSe symmetric double quantum wells

Nacir Tit[1,2,3] **and Ihab M Obaidat**[2]

[1] Abdus Salam International Center for Theoretical Physics, Strada Costiera 11, I-34100 Trieste, Italy

[2] Physics Department, UAE University, PO Box 17551, Al-Ain, United Arab Emirates

E-mail: ntit@uaeu.ac.ae

Received 1 January 2008, in final form 28 February 2008
Published 31 March 2008
Online at stacks.iop.org/JPhysCM/20/165205

Abstract

The bound states in the $(CdSe)_{N_w}(ZnSe)_{N_b}(CdSe)_{N_w}$–ZnSe(001) symmetric double quantum wells are investigated versus the well width (N_w) and the barrier thickness (N_b). A calculation based on the sp^3s^* tight-binding method which includes the spin–orbit interactions is employed to calculate the bandgap energy, quantum-confinement energy, and band structures. The studied systems possess a vanishing valence-band offset (VBO = 0) in consistency with the well known common-anion rule, and a large conduction-band offset (CBO $\simeq$ 1 eV), which plays an essential role in the confinement of electrons within the CdSe wells. The biaxial strain, on the other hand, plays another role in confining the holes at the interfaces (within the well regions) and thus enhancing the radiative efficiency. The induced-strain energy is estimated to be $\sim$35 meV. More importantly, the results show that, for a fixed barrier thickness, the double wells are able to confine a pair of bound states when they are very thin. By increasing the wells' width (N_w), further, a new pair of states from the conduction-band continuum falls into the wells every time N_w hits a multiple of four monolayers (more specifically, for $4n < N_w \leqslant 4(n+1)$, the number of bound states is $2(n+1)$, where n is an integer). On the other hand, the barrier thickness (N_b) is shown to have no effect on the number of bound states, but it solely controls their well-to-well interactions. A critical barrier thickness to switch off these latter interactions is estimated to occur at about $N_b^{crit} \simeq 9$ ($L_b^{crit} \simeq 25$ Å). Rules governing the variation of the quantum-confinement energy versus both barrier thickness (N_b) and well width (N_w) have been derived. Our theoretical results are also shown to have excellent agreement with the available experimental photoluminescence data.

1. Introduction

Over the last two decades, semiconductor physics has developed towards studies of low-dimensional systems which have been possible to synthesize due to the advent of modern growth techniques, such as molecular-beam epitaxy (MBE). Yet II–VI compound semiconductors have not undergone as many investigations as those devoted to III–V compounds, for which numerous applications have been realized, and have long seemed prone to remain embryonic. However, the recent achievement of p-type doping of ZnSe by MBE, followed by the realization of II–VI based blue-light emitters [1], has revived the interest in II–VI compounds. Moreover, the constant progress in epitaxial crystal-growth techniques, such as the development of flow-rate-modulated beam epitaxy and others, has made it possible to grow high-quality semiconductor heterostructures even from heavily lattice-mismatched materials (up to a lattice mismatch of $\sim$7%). As long as the strained slabs are kept sufficiently thin, the novel growth techniques have even explored the strain effect in the engineering of the heterostructure's bandgap to make it suitable for specific optoelectronic applications.

Among the II–VI compound semiconductors, the family Zn(Cd)Se(S) has attracted enormous interest for several reasons: to mention a few, for instance, (i) it possesses a variety of *direct* bandgaps covering most of the visible spectrum ranging from near infrared to ultra-violet [2], (ii) it is characterized by bright emissions and (iii) the lattice constants of ZnS, ZnSe and CdSe respectively match those of

[3] Author to whom any correspondence should be addressed.

Si, GaAs and InAs, which are popularly used as substrates. Thus many of its elements are easy to use as buffers. As a particularity in this family, ZnSe remains unique and broadly used as a buffer on GaAs because it has also a *direct* and large bandgap lying within the blue spectral region. When ZnSe–CdSe are combined and fabricated in heterostructures, they yield excellent emission and absorption properties suitable for green–blue photonic devices [3]. Nonetheless, any heterostructure made using elements of the family would be hampered by the combined effects of lattice mismatch (which is about 7% in case of CdSe/ZnSe) and cation diffusion at the interfaces [4]. Strain can place severe restrictions on the heterostructures that should be grown if lattice relaxation is to be avoided. The strained layer will relax towards its unstrained lattice parameter when it exceeds a certain critical thickness d_c, corresponding to the misfit dislocations to be nucleated at the interfaces. Such a critical thickness was estimated by Parbrook and co-workers [5] and Zajicek and co-workers [6] to be about $d_c \sim 1.3$ nm. It is due to these restrictions that nearly exclusively superlattices (SLs) mostly containing either the alloy (Cd, Zn)Se or ultra-thin CdSe slabs have been studied to avoid appearance of misfit dislocations.

The novel sophisticated epitaxial layer-growth techniques, such as self-limiting monolayer epitaxy (SME) [6], have paved the way for the fabrication of several new types of high-quality semiconductor heterostructures. Among these structures, single and double quantum wells (SQWs and DQWs) have been attractive because of the interest in the investigation of both fundamental physics properties [7] and tunable coherent-light sources for optical communications [8], besides having a good control on the charge distribution and the strain morphology. Using the SME, Zajicek and co-workers have succeeded in synthesizing high-quality CdSe single quantum wells in ZnSe [6]. They reported high photoluminescence peaks for CdSe wells of thicknesses 1–4 monolayers (MLs) and deduced the evidence of appearance of misfit dislocations in the case of a 5 ML single-well structure. In a subsequent related experimental work, Yamaguchi and co-workers [9] reported another successful growth of the CdSe SQWs in ZnSe using just MBE. They also showed that their PL study gives evidence for the localization of excitons to occur only due to interface roughness and well-width fluctuations. In a more recent work, Tu and co-workers [10] reported, for the first time, a successful growth of strained $Zn_{0.79}Cd_{0.21}Se$/ZnSe double quantum wells, grown by MBE on (001) GaAs substrate and using contactless electro-reflectance (CER) at both 15 and 300 K. Their CER spectra were compared to the results obtained using the envelope-function calculations, and the conduction-band offset (CBO) was estimated to be large, about 0.67 ± 0.03. The coupling between the CdSe DQWs was not in the scope of their investigation, as for many other studies. Nevertheless, the coupling between CdSe/ZnSe self-assembled quantum dots (QDs) appeared in some extended detail in the work of Kim and co-workers [11]. The decoupling was shown to be mainly controlled by the ZnSe barrier thickness.

On the theoretical side, several computational techniques were used to calculate the band structures of semiconductor heterostructures. However, many were limited either by the system size and the applicability only for ground-state properties (with underestimation of bandgap), such as the *first-principle* methods, or the complete neglect of the band-mixing effects, such as the effective-mass approaches (based on the Kronig–Penney model) and the Hückel method. To overcome such difficulties, we have used the sp^3s^* tight-binding (TB) method with inclusion of spin–orbit interactions [12–14], which are crucially important in the case of II–VI materials. The TB method has proven its reliability to successfully simulate the experimental data while it incorporates the microscopic description of the material, where the point-group symmetry of the system is included. Within the Slater–Koster scheme [15], the TB method uses a small basis set of atomic orbitals and this gives the method the ability to deal with large systems; meanwhile, it takes into account the band-mixing effects that are essential in the band structures of systems such as superlattices, quantum wires, dots and wells. It is worthwhile to emphasize, here, that such tasks can also be tackled by empirical pseudo-potential (EPP) methods, using either plane waves [16] or Bloch wavefunctions [17]. Such latter developed EPP methods achieved even the ability to deal with large systems containing of the order of 2000 atoms in their computational supercells. In addition to the computational task, we would emphasize one special striking feature of II–VI common-anion heterostructures, which is the vanishing or the very small value of the valence-band offset (VBO). This makes the mixing of valence bands even more essential, and the interplay between the biaxial strain (in the case of lattice-mismatched structures) and the vanishing VBO is of interest in its own right. We emphasize that in the case of lattice-mismatched heterojunctions there are ways to incorporate the biaxial strain effect, for instance, as a perturbation *posteriorly* added to the Hamiltonian within the TB scheme [13, 14].

In this present work we employ the sp^3s^* tight-binding models, with inclusion of the spin–orbit interactions, to investigate the electronic band structures of the $(CdSe)_{N_w}(ZnSe)_{N_b}(CdSe)_{N_w}$–ZnSe(001) symmetric double quantum wells (DQWs). We present the calculations of the bandgap energy, quantum-confinement energy and band structures of these DQWs versus the barrier thickness (N_b) and well width (N_w). The aim of the work will be the following: (i) to study the coupling behaviors of the symmetric DQWs and its characters; (ii) to derive the rules governing the variation of quantum-confinement energy versus both barrier and well widths; (iii) to predict the transition from coupled to uncoupled DQWs and to estimate the critical ZnSe barrier thickness for its occurrence and (iv) to show simulations of our theoretical results for some available PL data.

This paper is organized as follows. The next section gives to some extent the details of the TB models and method. In section 3, we discuss our obtained theoretical results and compare them to some available PL data. The last section summarizes our main findings and conclusions.

2. Computational method

The empirical TB method has been successfully used in several areas of solid state physics for many years [12–15], [18–20].

Within the TB framework, atomic levels and electronic-interaction integrals are actually taken as adjustable parameters in order to fit the experimental or the first-principle band structures. Vögl *et al* [18] have proposed a nearest-neighbor TB description of IV and III–V semiconductors using the sp^3s^* basis set. In their work, the actual Hamiltonian is replaced with a pseudo-Hamiltonian which involves five orbitals per atom: s and 3p orbitals to describe the sp^3 hybridization and one excited s^* orbital, whose function is to provide a better description of the lower unoccupied energy levels (low-lying conduction bands (CBs)). The first extension to further incorporate the spin–orbit coupling within the TB framework was done for II–VI materials, even prior to Vögl's work, by Kobayashi *et al* [12], namely on CdTe and HgTe. Of course, in these latter materials, the spin–orbit splitting is quite strong and its successful incorporation into the TB Hamiltonian has paved the way for a huge field of applications, especially in the area of II–VI materials. In addition to this extension, one reliable method to further include the strain effects in the TB calculations has been published by Bertho *et al* [13], where the strain has been treated as a perturbation *posteriorly* added to the TB Hamiltonian.

Here, in this paper, we use the empirical TB parameters, published by Olguin and Baquero [19] (shown in table 1), which yield excellent fittings to the experimental bandgaps and effective masses (see table 2, where the overall agreeable comparison to experimental data [21] is shown. Other methods yield results of effective masses very much scattered; see, for instance, [22]). The TB Hamiltonian matrix elements are expressed in a basis of symmetrically orthonormalized atomic orbitals (so-called Löwdin orbitals [20]). Moreover, in the supercell calculations, the validity of two main points is assumed: (i) the macroscopic theory of elasticity (MTE) [23] in evaluating the supercell atomic structure and (ii) the problem of energy reference between the two constituents is sorted out by taking the VBO into account [14] (for instance, in our present case, CdSe on-site energies are shifted up by the VBO since the valence-band (VB) edge of this constituent is always higher in energy than that of ZnSe when the interface is formed between them). Furthermore, it is worthwhile to mention that here in all the situations (unless indicated otherwise) we used VBO $= 0$, which was shown/justified in our previous work [24] to yield excellent fittings to PL data of CdSe/ZnSe SLs, besides the fact that this is also consistent with the famous common-anion rule.

With the inclusion of the spin–orbit interaction, the sp^3s^* TB Hamiltonian is expressed in the Löwdin basis set as follows:

$$H_{\rm so} = \sum_{i,\mu} E_{i,\mu}|i,\mu\rangle\langle i,\mu| + \sum_{i,\mu;\,j,\nu(i\neq j)} |j,\nu\rangle U_{i\mu,j\nu} e^{i\vec{k}(\vec{r}_j-\vec{r}_i)}\langle i,\mu| \quad (1)$$

where i and j refer to atoms at the respective positions $\vec{r}_i$ and $\vec{r}_j$; μ and ν refer to one of the ten orbitals on the atom i and j respectively; $E_{i,\mu}$ is an on-site (diagonal) energy element of orbital μ of site i and $U_{i\mu,j\nu}$ is the overlap integral between the indicated respective orbitals. For further details of the expressions of the overlap integrals, we refer the reader to reference [12], whereas the TB parameters are obtained from the work of [19].

It is worthwhile to mention that, before diagonalizing the Hamiltonian (1), it is extremely important to take care about crystal symmetry considerations; namely the existence of an inversion symmetry with respect to the planar-spin-averaged charge density (see the appendix).

The Bloch wavefunction $|n\mathbf{k}\rangle$, of course, should diagonalize the TB Hamiltonian and is written as

$$H_{\rm so}|n\mathbf{k}\rangle = E_{nk}|n\mathbf{k}\rangle \quad (2)$$

where n is a band index, $\mathbf{k}$ is a wavevector, usually taken either from within the irreducible wedge of the Brillouin zone if the aim is to calculate the density of states or along the high-symmetry lines if the aim is to calculate the bands, and E_{nk} is the eigenenergy corresponding to the eigenvector (Bloch wavefunction). In our particular case, both constituents possess *direct* bandgaps at the Γ point. So, with the exception of band structure calculations, the bandgap energy ($E_{\rm g}$) and the quantum-confinement energy ($E_{\rm Q}$) are calculated at the Γ point.

Last, but not least, we will also give a brief description of how the quantum-confinement energy is calculated. So, as the heterojunction made of CdSe/ZnSe is considered to be of type I, then the total charge-carrier quantum-confinement

Table 2. The calculated bandgap energies ($E_{\rm g}$ in eV) and carrier effective masses ($m_{\rm e}^*$, $m_{\rm HH}^*$ and $m_{\rm LH}^*$ in units of free-electron mass and along the [100] direction) are compared to the experimental data of [21].

Compound	$E_{\rm g}$	$m_{\rm e}^*$	$m_{\rm HH}^*$	$m_{\rm LH}^*$	$E_{\rm g}$ [a]	$m_{\rm e}^*$ [a]	m_h^* [a]
CdSe	1.78	0.126	0.609	0.158	1.75	0.11	0.44
ZnSe	2.83	0.443	0.774	0.344	2.83	0.16	0.60

[a] Experimental data due to [21].

Table 1. The empirical sp^3s^* TB parameters, with the inclusion of the spin–orbit coupling, for ZnSe and CdSe are in units of eV. The same notation as in [12] is used. The lattice constants (a_0) are in Å.

Compound	E_s^a	E_p^a	E_s^c	E_p^c	E_{s*}^a	E_{s*}^c	λ_a	λ_c
ZnSe	−12.427	1.782	0.047	5.520	7.850	0.194	0.194	0.019
CdSe	−10.167	1.034	1.080	7.646	6.027	3.962	0.143	0.067
Compound	a_0	$4V_{ss}$	$4V_{xx}$	$4V_{xy}$	$4V_{sp}^{ac}$	$4V_{ps}^{ac}$	$4V_{s*p}^{ac}$	$4V_{ps*}^{ac}$
ZnSe	5.65	−6.502	3.309	5.412	1.137	−5.802	3.266	−1.870
CdSe	6.05	−2.892	3.013	5.730	2.16	−5.656	2.116	−2.217

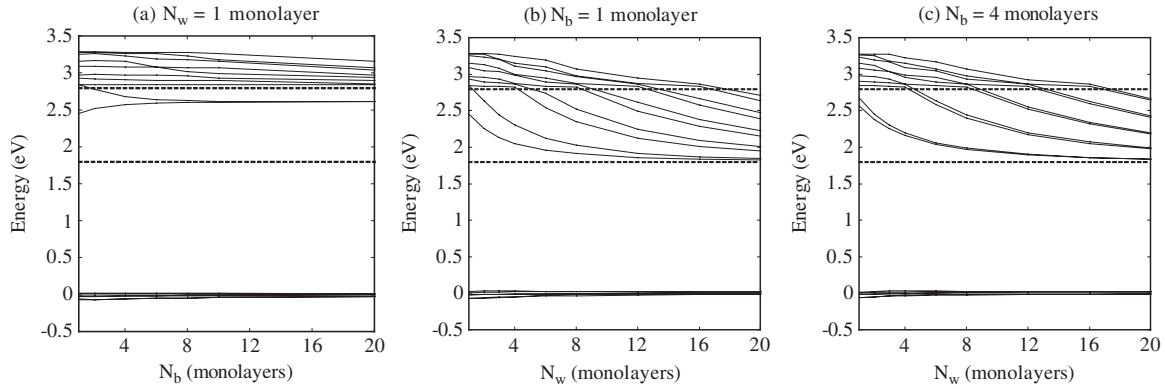

Figure 1. Theoretical results of variation of the lowest ten spin-degenerate CB eigenenergies and the highest six spin-degenerate VB eigenenergies of a $(CdSe)_{N_w}(ZnSe)_{N_b}(CdSe)_{N_w}$–ZnSe(001) DQW versus (a) barrier thickness N_b with $N_w = 1$, (b) well width N_w with $N_b = 1$ and (c) well width N_w with $N_b = 4$. VBO = 0 was taken in all these calculations. The region between the dashed horizontal lines corresponds to the CdSe well's energy region.

energy can be defined as $E_Q = E_g(SL) - E_g(CdSe)$, where $E_g(SL)$ is the bandgap energy of the whole system obtained from the supercell calculation, and $E_g(CdSe)$ is the bandgap energy of the pure CdSe in its strained configuration corresponding to the one existing in the supercell. Another method which would yield the same result, and which as a matter of fact was used in our present work, is as follows: for the $(CdSe)_{N_w}(ZnSe)_{N_b}(CdSe)_{N_w}$–ZnSe(001) DQW structure, we define the quantum-confinement energy as

$$E_Q = E_g(N_w, N_b) - E_g(N_w \to \infty, N_b) \qquad (3)$$

where $E_g(N_w, N_b)$ is the bandgap energy of the supercell which contains the two symmetric wells of N_w ML of CdSe each, and $E_g(N_w \to \infty, N_b)$ is the hypothetical bandgap of the same previous structure but where the wells' widths are infinitely broadened in order to let the ground state asymptotically touch the bottom of the wells. Computationally, we have found that it is sufficient to achieve this convergence by just letting $N_w \to 50$, which is easily affordable in our TB method.

The supercell $(ZnSe)_{20}(CdSe)_{N_w}(ZnSe)_{N_b}(CdSe)_{N_w}(ZnSe)_{20}(001)$, with periodic boundary conditions and containing $2(40+2N_w+N_b)$ atoms, and strained to ZnSe substrate, is used to simulate the symmetric $(CdSe)_{N_w}(ZnSe)_{N_b}(CdSe)_{N_w}$–ZnSe (001) double-quantum-well systems. Moreover, as both constituents have direct bandgap energies at the Γ-point, all the calculations (except the bands) are carried out at the Brillouin zone center. The results will be discussed next.

3. Results and discussion

Figure 1 displays the results of six valence-band and ten conduction-band eigenenergies calculated at the center of the Brillouin zone for the $(CdSe)_{N_w}(ZnSe)_{N_b}(CdSe)_{N_w}$–ZnSe double quantum well systems. All the displayed eigenstates are spin degenerate and the VB edge of the bulk constituents is taken as an energy reference. VBO = 0 is taken in all the calculations and consequently the CBO is estimated to be large (CBO $\simeq$ 1 eV) and forms a well for electrons, as shown by the region in between the two horizontal dashed lines, located at the energy range $1.80 \leqslant E \leqslant 2.80$ eV. Panel 1(a) shows the variation of the above eigenenergies versus the barrier thickness (N_b) when the wells' width is kept very small and equal to one monolayer ($N_w = 1$). Panel 1(a) shows that the ultra-thin CdSe wells are able to confine one pair of (spin-degenerate) bound states and these two states are strongly split when the barrier thickness (N_b) is small. This pair gets close in energy as the barrier thickness increases until they merge to have the same energy as a consequence of their well-to-well interaction being switched off; however, they become split in space into two independent single quantum wells. The critical barrier thickness corresponding to the coupled-to-uncoupled transition is estimated to occur at about $N_b^{crit} \simeq 9$ ML (i.e. $L_b^{crit} \simeq 25$ Å). The bandgap energy of the ultra-thin uncoupled/isolated wells (when $N_b > 9$) is found to be $E_g = 2.60$ eV, which corresponds to a quantum-confinement energy $E_Q = 0.80$ eV. In the same panel 1(a), one may also notice the split of top valence-band states especially when N_b is small as a result of the compressive biaxial strain applied on the CdSe wells. The CdSe-related heavy-hole (HH) state represents the top of VB states as the wells are compressively strained. On the other hand, in panels 1(b) and (c), the variations of the eigenenergies versus the wells' width are shown for two different barrier thicknesses, $N_b = 1$ and 4 respectively. While the VB states are shown to keep behaving similarly to panel 1(a), the CB states behave in a completely different way. Namely, in panel 1(b), when the wells are thin ($N_w \leqslant 4$), only one pair of (spin-degenerate) bound states exists in the wells. As the wells' width (N_w) increases, a new pair among the CB continuum states falls into the wells every time N_w hits a multiple of four (precisely, for $4n < N_w \leqslant 4(n+1)$ the number of (spin-degenerate) bound states is $2(n+1)$, where $n = 0, 1, 2, 3, \ldots$, etc). This rule might be attributed to the inversion-symmetry requirement, which was imposed on the wavefunctions in order to be elegible to form a new venter inside the CdSe well. It seems that the smallest possible space to accommodate the smallest venter must be of two-unit-cell length along the c-direction. A further remark about panel 1(b) is that the noticeable band-mixing (crossing), occurring among

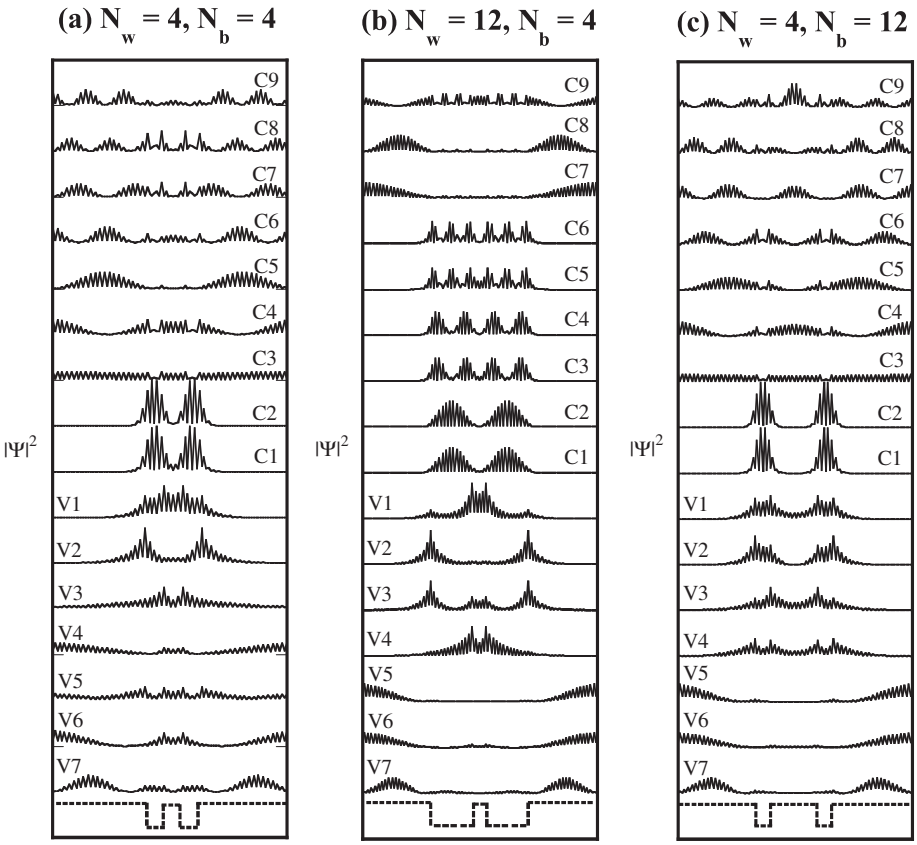

Figure 2. The planar spin-averaged wavefunction-squared amplitudes of the highest seven VB states and lowest nine CB states are shown along the *c*-axis. The dashed lines corresponding to the CB-edge profile are shown as guides to the eye. The three panels correspond to $(\mathrm{CdSe})_{N_\mathrm{w}}(\mathrm{ZnSe})_{N_\mathrm{b}}(\mathrm{CdSe})_{N_\mathrm{w}}$–ZnSe(001) DQWs with (a) $N_\mathrm{w} = 4$, $N_\mathrm{b} = 4$, (b) $N_\mathrm{w} = 12$, $N_\mathrm{b} = 4$ and (c) $N_\mathrm{w} = 4$, $N_\mathrm{b} = 12$.

the continuum CB states above the wells as N_w is varied, indicates that the states falling into the wells must have certain specifically selected symmetry. This is similar to the mixing effects reported in [17]. By comparing panel 1(b) to panel 1(c), one can clearly notice that the pair of (spin-degenerate) states falling into the wells in panel 1(c) is much closer in energy to each other. This is the case because in panel 1(c) the barrier is thicker and the wells are more separated so that the split energy is smaller. Meanwhile, one also notices that all the pairs of bound states shown in both panels 1(b) and (c) are split in energy, an indication that the wells are interacting (coupled) as long as the barrier thickness is still smaller than $L_\mathrm{b}^\mathrm{crit}$ (i.e. $N_\mathrm{b} < 9$).

Figure 2 shows the wavefunction-squared amplitudes of the spin-averaged eigenstates ($|\Psi|^2 = \frac{1}{2}(|\Psi_\uparrow|^2 + |\Psi_\downarrow|^2)$), calculated at the Γ point, versus the Z-direction (layer by layer) for seven VB states and nine CB states. The dotted curve at the bottom of each panel displays the profile of the CB edge. First, we discuss the behaviors of the holes (top VB states). One common trend between all panels of figure 2 is the localization of holes at the interfaces, i.e. in the neighborhood of the wells, as an effect of the biaxial strain imposed on the CdSe wells. This is similar to the PPM results reported by Gell and co-workers [25], who illustrated the existence of confined states in the absence of band offset. Panel 2(a), where $N_\mathrm{w} = 4$ ML and $N_\mathrm{b} = 4$ ML, shows the confinement of three holes (V1–V3), whereas the other lower VB states are basically delocalized and just constituting the VB continuum (this particular case may be considered as similar to the alloying regime; see the next figure for more details). It seems that the biaxial strain has induced small wells. (There are basically four hidden wells, each at one interface and hereafter named 'h-wells', see their effects in the other panel as well. Note that these h-wells are not necessarily square in shape.) Panel 2(b) gives more details: if the wells' thicknesses are simultaneously increased to $N_\mathrm{w} = 12$ ML, then the h-wells have enough strain energy to confine four holes (V1–V4) at the interfaces, and four other states (V5–V8, note that V8 is not shown here) are also competing to enter the h-wells but just could not make it as these 'hidden' interface h-wells are small in both energy and space. So these four VB states (V5–V8) remain frustrated and pending at the gates of the h-wells. The rest of the VB states (below V8, not shown) are found just to be delocalized. Panel 2(c) also shows the localization of the top four holes (V1–V4) at the interfaces whereas the next VB states (V5–V8) are also competing to enter the h-wells but just got repelled as there is no space in there to accommodate them. The other VB states (below V8 not shown here) are found to be all extended.

Second, in figure 2, we discuss the behaviors of CB states, which are really shown to follow completely different profiles. Their wells are large (of depth equal to CBO $\simeq$ 1 eV; there are basically two wells for the electrons, named hereafter 'e-wells'). They are mainly sensitive to the variation of the wells'

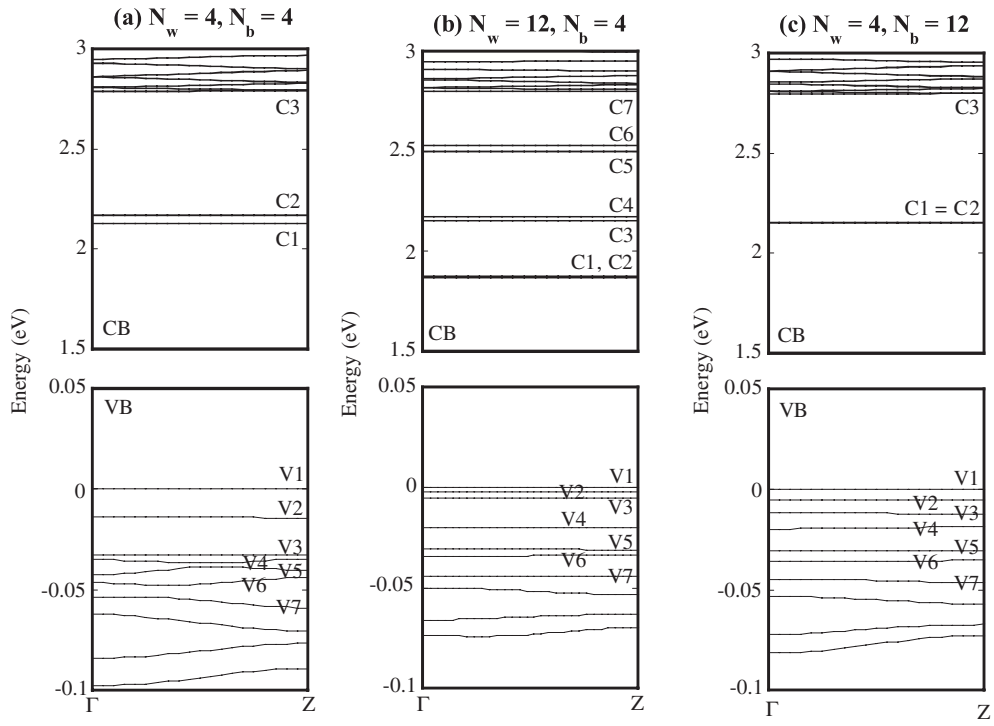

Figure 3. The band structures of $(CdSe)_{N_w}(ZnSe)_{N_b}(CdSe)_{N_w}$–ZnSe(001) DQWs are shown along the ΓZ high-symmetry line for (a) $N_w = 4$, $N_b = 4$; (b) $N_w = 12$, $N_b = 4$; (c) $N_w = 4$, $N_b = 12$. The VB edge of the supercell is taken as an energy reference and the sub-panels show the VBs and CBs separately for the purpose of clarity.

width (N_w). For instance, when $N_w = 4$ ML, the wells are able to confine only one pair of (spin-degenerate) bound states (see C1 and C2 in panels 2(a) and (c)); the other upper CB states are basically delocalized as constituting part of the continuum states. In panel 2(b), the wells' width is increased to $N_w = 12$ ML while N_b is kept constant, $N_b = 4$ ML; three pairs of bound states have entered the e-wells. It is worth to emphasize, here, the successful implementation of the inversion symmetry inside the TB Hamiltonian (see the appendix), such that the electronic bound states within the CdSe wells, shown in figure 2, look well behaved, as can be predicted by the application of quantum theory on a single particle in a finite quantum well (i.e., C1 and C2 have one venter inside each well as the ground states, C3 and C4 have two venters inside each well as the first excited states; C5 and C6 have three venters inside each well as the second excited states). More importantly, the two lowest CB continuum states at the top of the wells (just above C6 in panel 2(b)) look as if they are more localized in the ZnSe regions away from the wells. This is another quantum mechanical effect imposed by the wells' symmetry rules to prohibit these latter states landing in the wells. So these two latter states become like frustrated states, being at the threshold to be allowed to enter the wells; more precisely, they just get reflected from the wells' region as rejected. Thus, the two CB states (just above C6 in panel 2(b)) keep pending at the gates of the e-wells. In contrast to this, the other upper CB states are delocalized as part of the CB continuum states.

Figure 3 displays the band structures corresponding to the three structures of figure 2 in respective panels. Only one high-symmetry line (ΓZ) is displayed to study the confinement effects and both the CBs and VBs are shown but in different respective sub-panels. All the shown bands are spin degenerate. The VB edge is taken as an energy reference and similar energy scales are used for all three panels to ease the comparison. The scale of the VB sub-panels is small for the purpose of clarity. As discussed and shown in figure 1, the e-wells' energy range is from 1.8 to 2.8 eV as the CBO $\simeq$ 1 eV. First we discuss the CB sub-panels: panel 3(a), where $N_w = 4$ ML and $N_b = 4$ ML, shows the existence of one pair of (spin-degenerate) bound states as clearly displayed by the flat bands (C1 and C2). Such confinement behavior corroborates what was demonstrated before in figures 1 and 2. The bound states are split in energy as an effect of the active well-to-well interaction as the barrier is thin ($N_b < 9$ ML). In panel 3(c), the enlarging of the barrier thickness (to $N_b = 12$ ML) can only affect the split energy, not the number of bound states. The pair of states merges, in terms of energy, into one degenerate state (panel 3(c)), but is split again in the direct space into two independent wells. Panel 3(c) confirms that the wells are decoupled and also corroborates the fact that $N_b > 9$ ML corresponds to a situation of decoupled wells. In panel 3(b), the wells' width is increased to $N_w = 12$ ML while the barrier thickness is kept similar to panel 3(a) ($N_b = 4$ ML), so that the wells are able to accommodate three pairs of (spin-degenerate) bound states (C1–C6).

One common feature between the three CB sub-panels of figure 3 is the fact that almost all the CB states above the wells' region ($E \geqslant 2.8$) are shown to be dispersive because they are delocalized and constituting part of the CB continuum. One

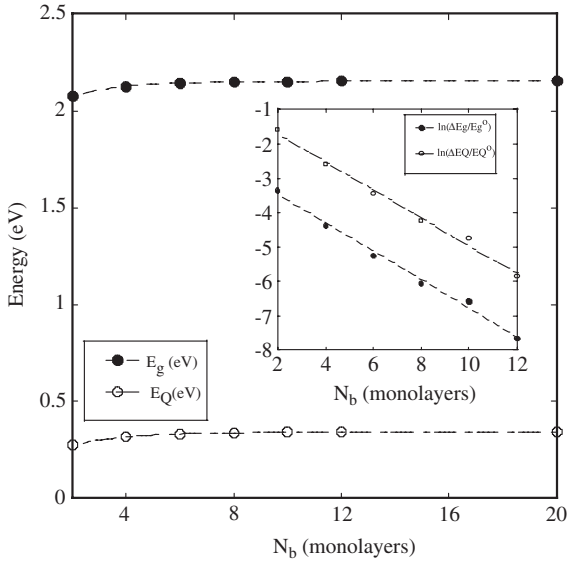

Figure 4. The bandgap energy E_g (full circles) and quantum-confinement energy E_Q (open circles) of the CdSe–ZnSe DQWs are shown versus barrier thickness (N_b). $N_w = 4$ was taken. The inset shows the variation of $\ln(\Delta E_g/E_g^0)$ in solid circles and $\ln(\Delta E_Q/E_Q^0)$ in open circles versus N_b.

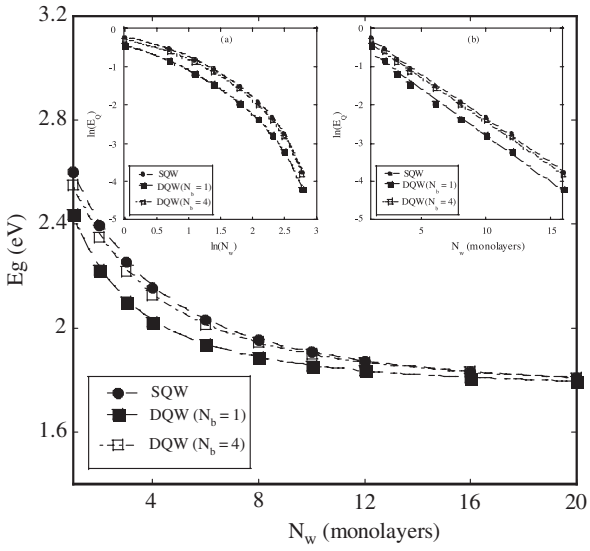

Figure 5. The bandgap energies of a CdSe–ZnSe SQW (full circles), a DQW with $N_b = 1$ (full squares), and a DQW with $N_b = 4$ (open squares) are shown versus well width (N_w). Inset (a) shows the log–log variation of E_Q, whereas inset (b) shows the semi-log variation of E_Q.

further remark about the CB sub-panel 3(b) is that the higher-energy pairs of localized states within the CdSe wells are a bit more split in energy because the wells are still coupled (as the barrier is thin $N_b < 9$ ML); furthermore, the split energy increases when going from the lower-energy to the upper-energy bound states as an effect of the increase of the coupling strength. Now about the VB sub-panels of figure 3: 10 VBs are displayed and confirm that the top three VBs (V1–V3), at least, in all the panels are localized as their corresponding bands are 'flat'. Furthermore, in panel 3(a), the lower bands (V4 and below) are shown to be dispersive and should constitute part of the VB continuum. Some bands (such as V4 and V5 in panel 3(a)) exhibit some inter-band mixing, which reveals the active coupling between the wells (almost the same as the alloying regime). The V3 state seems to have an energy at the level of the gate of the h-wells (35 meV), below which the VB states are extended. In the VB sub-panel 3(b), where the well width is increased to $N_w = 12$ ML while the barrier thickness is kept the same as in panel 3(a) ($N_b = 4$ ML), the energy confinements of the holes reduce in their strain-induced wells (h-wells) which, in turn, could accommodate even more hole bound states (see V1–V4, all being 'flat'). In the VB sub-panel 3(c), where the well width is similar to panel 3(a) ($N_w = 4$ ML) and the barrier thickness is increased to $N_b = 12$ ML, the wells are completely decoupled and the interfaces could accommodate just four hole bound states (V1–V4 in panel 3(c)). The states V5 and V6 are located at the gate of the h-wells, in terms of energy (31–35 meV), below which VB states are extended. Thus, the confinement behaviors of the holes also reveal the formation of induced wells (hidden) at the interfaces to accommodate holes at the well regions. The estimated depth of these h-wells is about 35 meV. It is interesting to note that in the input we have used VBO = 0, and as a result of the biaxial strain exerted on the CdSe wells we obtained a small strain-induced $\mathrm{VBO_{ind}}(\simeq 35$ meV), which is of the order of strain energy. This phenomenon is also consistent with the findings of the pseudo-potential calculations reported in [25].

To investigate the rules governing the variation of either the bandgap energy (E_g) or the quantum-confinement energy (E_Q), we first display in figure 4 the variation of both of these latter quantities versus the barrier thickness (N_b), while the wells' width is kept constant ($N_w = 4$). By increasing the barrier thickness (N_b), both E_g and E_Q (in full circles and open circles respectively) increase to reach their corresponding values obtained for the separate single quantum wells (SQWs). Beside the fact that the tendency to this is so rapid, one expects the variation to be like an exponential one which follows the form of evanescent wavefunctions in penetrating the barrier. So, in the inset of figure 4, we plotted both $\ln(\Delta E_g/E_g^0)$ and $\ln(\Delta E_Q/E_Q^0)$ versus the barrier thickness (N_b), where in $\Delta E_g = E_g - E_g^0$, E_g and E_g^0 correspond to the bandgap energies of the DQW and SQW respectively; and similarly in $\Delta E_Q = E_Q - E_Q^0$, E_Q and E_Q^0 correspond to the quantum-confinement energies of the DQW and SQW, respectively. It turned out that the curves shown in the inset are really linear, confirming that the variation is indeed exponential. So, we deduced that one can write the following rules:

$$E_g^{\mathrm{DQW}} = E_g^{\mathrm{SQW}}\left[1 - \exp\left(-\frac{L_b}{\xi_b}\right)\right] \tag{4}$$

$$E_Q^{\mathrm{DQW}} = E_Q^{\mathrm{SQW}}\left[1 - \exp\left(-\frac{L_b}{\xi_b}\right)\right] \tag{5}$$

where $L_b = \frac{1}{2}N_b a_0(\mathrm{ZnSe})$. The two curves in the insets are shown to be parallel, having the same slope, so both E_g and E_Q are found to possess the same characteristic length $\xi_b \simeq 6.5$ Å.

In figure 5, we display the variation of the SQW (in full circles), the DQW with $N_b = 1$ (in full squares), and the DQW with $N_b = 4$ (in open squares) versus the wells' width (N_w). The ground state in all the three cases seems to fall down to the bottom of the well as these latter get wider. Of course, the ground state will never reach the bottom of the well as an optimum kinetic energy is needed to keep the particle moving back and forth in the wells. At first, one would think that the quantum-confinement energy should decay in a power-law form similar to the case of an infinite well (where $E_Q \sim 1/L_w^2$). So, in inset (a), we have shown a log–log plot, namely $\ln(E_Q)$ versus $\ln(N_w)$, to access the validity of the power-law behavior. It turned out that this latter curve is not linear, so that E_Q does not follow a power-law variation (i.e. $E_Q \neq AL_w^{\alpha}$). In inset (b), moreover, we have plotted $\ln(E_Q)$ versus N_w. The three curves are found to be linear and parallel. So, by comparing the two insets of figure 5, one can easily conclude that the confinement energy is behaving more likely as an exponential decay rather than a power-law. Its variation is

$$E_Q = E_Q^0 \exp\left(-\frac{L_w}{\xi_w}\right) \tag{6}$$

where $L_w = \frac{1}{2}N_w a_0(\mathrm{CdSe})$; E_Q and E_Q^0 are the quantum-confinement energies of the SQW (or DQW) corresponding to the well widths of N_w monolayers and $N_w = 1$ ML respectively. The characteristic length is found to be the same as being dependent solely on the well's composition and equal to $\xi_w \simeq 13$ Å. This value is about twice ξ_b, indicating that the variation here is smoother. Moreover, this ξ_w value is half of the critical barrier thickness corresponding to the symmetric DQW decoupling. Thus, ξ_w may correlate to the localization length of the e/h-pair ground bound states.

On the experimental side, in order to avoid the appearance of misfit dislocations, the CdSe slabs must be kept thinner than 5 ML. For this reason, Zajicek and co-workers [6] have reported their photoluminescence results on MBE-grown CdSe SQWs of thicknesses less than 5 ML. As a matter of fact, they have grown two kinds of samples: (i) samples containing only one single well of CdSe (of thickness ranging from 1 to 3 ML) embedded inside ZnSe and called thereafter 'SQW' samples (the data are shown in figure 6 by full circles) and (ii) one sample containing five multiple quantum wells (MQWs) separated by identical ZnSe slabs of 300 Å thickness each, whereas the CdSe wells have thicknesses ranging from 1 to 5 ML in the respective order when moving from the substrate along the *c*-axis. The data are shown in figure 6 by open squares. Our calculated bandgap energy for the $(\mathrm{CdSe})_{N_w}$–ZnSe(001) SQW structures using both VBO = 0 and 0.3 eV is shown in figure 6 by dotted and solid curves respectively. We emphasize that the latter VBO value corresponds to the maximal bandgap energy that can be obtained using our TB models, and by coincidence it is also close to the one (0.33 eV) reported by Ren and co-workers [26], estimated using the state-of-the-art *ab initio* technique. For the three independent SQW samples, the theoretical results (solid line) agree with PL data (•) but a bit shorter with an energy difference of no more than 54 meV, such as in the case of 3 ML SQW-sample. This small energy shortage might be due to two reasons: the neglect of exciton effects in the TB calculations from the theoretical side and/or the problem of cation diffusion [4] at the interfaces from the experimental side. For the MQW sample containing five separate SQWs (where N_w = 1–5 ML), there is an excellent agreement with our theoretical results (dotted line) obtained with VBO = 0. Only the experimental SQW of $N_w = 5$ ML has a PL peak of low intensity and low energy lying below what the theory predicts. It is agreed by both theory and experiment that this latter SQW is considered, as it obviously contain misfit dislocations, and using this sample the critical well width corresponding to the nucleation of interface defects was estimated to be $N_w^{\mathrm{crit}} = 5$ ML, which is consistent with the prediction of Parbrook *et al* [5].

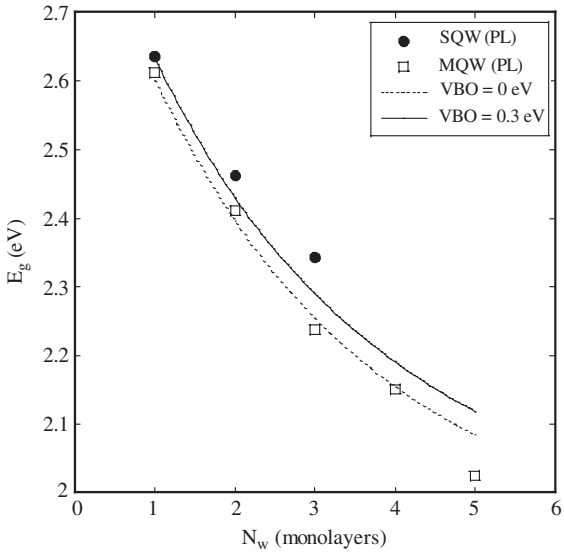

Figure 6. Photoluminescence data due to [6] obtained for a CdSe–ZnSe SQW (full circles) and MQW (open squares) versus well width N_w. The dotted and solid curves correspond to the TB results obtained for the SQW using the respective VBO = 0 and 0.3 eV.

4. Conclusions

The electronic structures of the $(\mathrm{CdSe})_{N_w}(\mathrm{ZnSe})_{N_b}(\mathrm{CdSe})_{N_w}$–ZnSe(001) symmetric DQWs were investigated using the sp^3s^* tight-binding method where the strain and spin–orbit effects are included. The bandgap energy, quantum-confinement energy and band structures were studied versus the barrier thickness (N_b) and well width (N_w). The results may be summarized as follows.

(i) Consistent with the common-anion rule, VBO = 0 was taken. Nonetheless, the results have shown that the CdSe-related HH still represents the VB top states and it always gets localized at the interfaces (near the well region), which yields high radiative efficiency. Moreover, the biaxial strain is able to form four small induced wells (named h-wells, each of depth of the order of the strain energy, ∼35 meV) to localize the top four holes at the interfaces (near the well regions).

(ii) The barrier thickness (N_b) has no effect on the number of electron bound states within the e-wells (each of the two wells is of depth CBO $\simeq$ 1 eV), but rather controls their well-to-well interaction. The transition from coupled to uncoupled DQWs is estimated to occur at a critical ZnSe barrier thickness of 9 ML (i.e. of about 25 Å).

(iii) The wells' width is the only parameter to control the number of electron bound states existing in the e-wells. The increase of well width (N_w) by multiples of four would admit a new pair of electron bound states to enter each time. The smallest bound-state wavefunction's venter requires a length of two unit cells along the c-axis to be accommodated. This was justified by a symmetry-selection rule. For the wells of thickness $4n + 1 \leqslant N_w \leqslant 4(n + 1)$ the number of bound states would be $2(n + 1)$, where $n = 0, 1, 2, 3, \ldots$ etc (an integer).

(iv) The rules governing the variation of quantum-confinement energy versus barrier thickness and well width were derived. Both variations were found to be exponentials.

(v) Our theoretical results of bandgap energies were found to be in excellent agreement with the available PL data of SQW and MQW, and indeed justify the reliability of our DQW predictions. Besides, these agreements with experiments have showed the relevance of our theoretical work in predicting the structural qualities and optical properties of the experimental samples.

(vi) As the experimental SQWs cannot be thicker than 4 ML, if misfit dislocations are to be avoided, then one should expect them to contain only one pair of electrons at a time regardless of the barrier thickness.

Acknowledgment

One of us (NT) benefited from a summer visit to the ICTP in Trieste (Italy) under the umbrella of the ICTP associateship program.

Appendix

For the cases of an SQW as well as a symmetric DQW, each structure possesses a point-group symmetry of high order, called hereafter inversion symmetry (as far as the planar-spin-averaged charge density ($\rho(z) = |\Psi(z)|^2$) is concerned). For instance, in the case of the $N_w = 1$ and $N_b = 1$ DQW, shown in Figure A.1, the inversion center of $\rho(z)$ would be the cation (Zn) located in the barrier. It should be further emphasized that in the case of N_b being odd the midway cation (Zn) of the barrier should be considered as an inversion-symmetry center, whereas in the case of N_b being even the midway anion (Se) of the barrier should be considered as an inversion-symmetry center. In figure A.1, the well width is $L_w = \frac{1}{2}N_w a_0(\text{CdSe})$, and the barrier thickness is $L_b = \frac{1}{2}N_b a_0(\text{ZnSe})$, where $a_0(\text{ZnSe}) = 5.65$ Å and $a_0(\text{CdSe}) = 6.78$ Å are the lattice constants corresponding to these respective materials as exist in the strained configurations of the supercell.

It is very important that such physical inversion symmetry should be translated into the Hamiltonian matrix representation. The way to do this is to change the order of the Hamiltonian basis set at the level of single atoms, namely by flipping the order of atomic orbitals of all the atoms located above the inversion-symmetry center. For instance, as shown in figure A.1, if the atoms below the inversion-symmetry center have arrows directed to the right then this indicates that the order of states goes as $|S1\rangle = |s, \uparrow\rangle$, $|S2\rangle = |s, \downarrow\rangle$, $|S3\rangle = |\frac{3}{2}, +\frac{3}{2}\rangle$, $|S4\rangle = |\frac{3}{2}, +\frac{1}{2}\rangle$, $|S5\rangle = |\frac{3}{2}, -\frac{1}{2}\rangle$, $|S6\rangle = |\frac{3}{2}, -\frac{3}{2}\rangle$, $|S7\rangle = |\frac{1}{2}, +\frac{1}{2}\rangle$, $|S8\rangle = |\frac{1}{2}, -\frac{1}{2}\rangle$, $|S9\rangle = |s^*, \uparrow\rangle$, and $|S10\rangle = |s^*, \downarrow\rangle$; then all the atoms above the inversion-symmetry center should have arrows directed to the left, indicating the reversal order of orbitals: i.e. their basis sets should start from $|S10\rangle$ and end at $|S1\rangle$ orbitals. For the atom considered as an inversion center, it would not really matter in what order its orbitals were put.

Finally, it is worthwhile to mention that the implementation of the inversion symmetry is necessary to obtain well behaved eigenwavefunctions as physically expected, but has no effect on the eigenenergies.

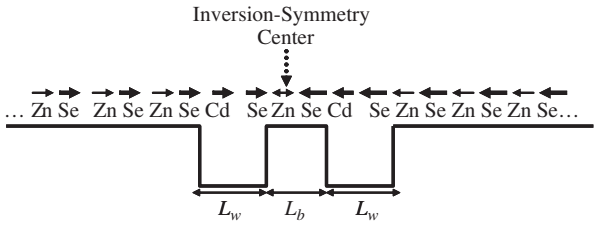

Figure A.1. CB-edge profile corresponding to the structure of a symmetric $(\text{CdSe})_{N_w}(\text{ZnSe})_{N_b}(\text{CdSe})_{N_w}$–ZnSe(001) DQW with $N_w = N_b = 1$. The arrows are used as an indication of the order of the basis set of orbitals on each atom. Note that this order is reversed for the atoms above the inversion-symmetry center (i.e. to the right of the center in the figure).

References

[1] For a review, see for instance, Neumark G F, Park R M and DePuydt M 1994 *Phys. Today* **47** 26
[2] Trager-Cowan C, Parbrook P J, Henderson B and O'Donnell K P 1992 *Semicond. Sci. Technol.* **7** 536
[3] Peng X 2006 *Nat. Mater.* **5** 923
[4] Parbrook P J *et al* 1991 *Semicond. Sci. Technol.* **6** 818
[5] Parbrook P J *et al* 1992 *J. Cryst. Growth* **117** 492
[6] Zajicek H *et al* 1993 *Appl. Phys. Lett.* **62** 717
[7] Feldman J *et al* 1987 *Phys. Rev. Lett.* **59** 2337
[8] Ogawa M and Mendez E E 1992 *Appl. Phys. Lett.* **60** 2971
[9] Yamaguchi S *et al* 1996 *Phys. Rev.* B **54** 2629
[10] Tu R C *et al* 1998 *J. Appl. Phys.* **83** 1043
[11] Kim T W, Yoo K H, Kim G H, Lee S, Furdyna J K and Dobrowolska M 2005 *Solid State Commun.* **133** 191
[12] Kobayashi A, Sankey O F and Dow J D 1982 *Phys. Rev.* B **25** 6367
[13] Bertho D, Jancu J M and Jouanin C 1994 *Phys. Rev.* B **50** 16956
[14] Tit N and Al-Zarouni A 2002 *J. Phys.: Condens. Matter* **14** 7835
[15] Slater J C and Koster G F 1954 *Phys. Rev.* **94** 1498
[16] Kurt A M and Zunger A 1994 *Phys. Rev.* B **50** 17393

[17] Ninno D, Wong K B, Gell M A and Jaros M 1985 *Phys. Rev.* B **32** 2700
[18] Vögl P, Hjalmarson H P and Dow J D 1983 *J. Phys. Chem. Solids* **44** 365
[19] Olguin D and Baquero R 1995 *Phys. Rev.* B **51** 16891
[20] Löwdin P O 1950 *Phys. Rev.* **18** 365
[21] Hellwege K-H (ed) 1982 *Landolt-Börnstein, New Series* vol 17b (Berlin: Springer)
[22] Rubio-Ponce A, Olguin D and Hernandez-Calderon I 2003 *Superficies Vacio* **16** 26
[23] Van de Walle C G 1989 *Phys. Rev.* B **39** 1871
[24] Tit N and Obaidat I M 2008 *Eur. Phys. J. Appl. Phys.* submitted
[25] Gell M A, Wong K B, Ninno D and Jaros M 1986 *J. Phys. C: Solid State Phys.* **19** 3821
[26] Ren Sh-F, Gu Zh-Q and Chang Y-C 1994 *Phys. Rev.* B **49** 7569